3rd Middle East Turbomachinery Symposium (METS III)
15-18 February 2015 | Doha, Qatar | mets.tamu.edu

REMAINING LIFE ASSESSMENT AND PERFORMANCE CHARACTERIZATION OF CENTRIFUGAL COMPRESSORS IN LNG TRAINS

Pradip B Sonavane
Senior Engineer (Rotating Equipment Engineering)

Atul W Deshpande
Head (Rotating Equipment Engineering)

RasGas Company Limited
Doha, State of Qatar

Thomas A. Chirathadam
Research Engineer

Harold R. Simmons
Technical Advisor

Southwest Research Institute
San Antonio, Texas, USA

Pradip Sonavane *is a Senior Engineer with Rotating Machinery in Technical Department at RasGas LNG Company, Qatar. He has core machinery experience of total 17 years at both Oil Refinery and LNG Plants. He started his career as Workshop Engineer in Oil Refinery (BPCL – Mumbai Refinery) for first 7 years, and then at Boiler House, CPP, and Hydro Carbon / LNG Processing Plants. He has authored and presented 2 Case Studies on the subject of Dry Gas Seals upgrade. Pradip has pursued his Masters in Management in 2005 from Mumbai University, India, and BE degree in Mechanical in 1997 from Shivaji University, Kolhapur, Maharashtra State, India (Walchand College of Engineering, Sangli).*

Atul Deshpande *is Head of Rotating Equipment Engineering with RasGas, Qatar. His responsibilities include machinery upgrades, surveillance, trouble shooting and long term reliability and availability improvement. Atul has over 25 years experience in Oil/Gas/LNG industry and has previously held engineering and asset management positions in PETRONAS, Malaysia and ONGC, India.*

Thomas Chirathadam *is a Research Engineer with the Fluids and Machinery Engineering Department at Southwest Research Institute in San Antonio, TX. He has experience in machinery dynamic analysis, rotordynamic analysis, and in fluid bearing design and testing. He has authored over 15 technical papers on the subject of turbomachinery dynamics, gas bearing performance, system parameter identification, remaining life analysis, and piping vibration control. Dr. Chirathadam received his Ph.D. and M.S. degrees (2012, 2009) in Mechanical Engineering from Texas A and M University, College Station, TX, and a B.S. degree (Mechanical Engineering, 2005) from the National Institute of Technology, Calicut, India.*

Harold Simmons *is a Technical Adviser at Southwest Research Institute providing technical support and guidance in machinery dynamics and failure analyses investigations of turbomachinery, gas turbines, and industrial fans for electric power and energy industry clients. For over 35 years, Harold has led numerous onsite failure analysis and turbomachinery troubleshooting investigations. He has developed protocols especially suited to diagnosing blade failure problems based on bench testing and generalized aerodynamic simulation. Harold is now focused on mentoring younger engineers in this field and on advancements in the wind turbine industry. Mr. Simmons is registered as a Professional Engineer in Texas and graduated from the University of Florida with a BSME in 1963.*

ABSTRACT

RasGas LNG Trains-1 and 2, comprising of three refrigeration centrifugal compressors each, were commissioned in 1999 and 2000, respectively. Three compressors have achieved 15 years of trouble free operation through risk based Predictive and Preventive Maintenance Strategies and surveillance program. None of these compressors' major components such as the rotor, dry gas seals or bearings have been replaced so far except three cases due to design upgrades (Rotor Re-rate, Thrust Disk fretting issue). Industry and technical literature survey indicates that several hundred compressors have achieved service life of over 20 years. However, the frequencies of maintenance interventions are not common/standardized due to site specific variations, shutdown

windows and differences in applications. In the LNG business, major maintenance activities of these compressors are required to be aligned with Gas Turbine Driver's 8 yearly Major-Inspection Cycles to avoid extended outages and very high adverse economic consequences. Train-1/2 compressors' running life would exceed 23 years, well beyond API recommended service life of 20 years, when the next Gas Turbine Major-Inspection (MI) is scheduled.

This Paper presents Engineering Studies on these six Compressors for the assessment of all potential failure modes, estimating remaining operational life and identifying requisite life-extension recommendations for meeting the challenge of achieving failure free operation for the extended period of 8 years. The compressor components are susceptible to low and high cycle fatigue, erosion, corrosion, creep, wear, and accumulated damages resulting in performance degradation and may eventually lead to failures. Review of rotor-dynamic design and performance, head/end wall O-ring life estimation, balancing drum condition review, and acoustic mapping were performed to evaluate the compressor train reliability and to benchmark the current system performance. To predict the static and dynamic stress distribution on compressor impellers (14 in total), detailed finite element (FE) models of the impellers are developed and validated using results from modal testing of spare impellers. The stress predictions using conservative estimates of alternating fluid pressure loads and rotor spin motion as forcing functions allow computing the impeller endurance limit, i.e., the stress limit corresponding to its infinite life. A stress based life prediction method, using Goodman diagram, was used to determine the impeller margin of safety.

Aerodynamic excitations and structural resonant vibrations mostly contribute to the acoustic emissions. Non-intrusive acoustic and vibration measurements were performed near the compressors and piping to benchmark the current operating condition of the system, which will serve for future Condition monitoring and periodic system evaluation. Rotordynamic response measurements from bode plot, waterfall plots, and orbit plots was reviewed to identify the rotor critical speeds, sub-synchronous whirl, rotor misalignment, and rubbing. The compressor efficiency and pressure ratios are characterized and trends developed to evaluate historic performance. This study for the assessment of the remaining life of centrifugal compressors provides a reference for development of long term maintenance philosophy for all RasGas LNG trains and gas processing plants.

INTRODUCTION

Remaining Life Assessment involves a set of analyses to estimate the useful residual life of machinery, identify probable failure modes, and recommend requisite life extension procedures with the objective of uninterrupted service beyond the OEM specified operating life. Thus, the primary objectives of performing these analyses are economic gain, reduced downtime, and reliable safe operation. The paper presents a study on the remaining life of six centrifugal compressors owned by RasGas and installed in LNG Trains 1 and 2 at RasLaffan Industrial city, Qatar. The refrigeration compression trains consist of three centrifugal compressors each: Mixed Refrigerant Low Pressure (MR-LP, 4 Stage MCL) compressor, Mixed Refrigerant High Pressure (MR-HP, 6 Stage BCL) compressor, and Propane (PR, 4 Stage MCL) compressor. The refrigeration compression strings are driven by GE Fr-7A Gas Turbines.

RasGas and Southwest Research Institute (SwRI) collaborated on a study to estimate the remaining life of these compressors, and to evaluate the viability of using the compressors for another 8 more years (crossing API 617 recommended life of 20 years) till next scheduled shutdown cycle in 2022 following Gas Turbine Driver's 8 yearly Major Inspection - by identifying potential failure modes.

As the refrigeration compressor trains are currently in operation following Train-1 and Train-2 major shutdowns in April-May 2014, there is no possibility of inspecting the compressor internal components. The remaining life assessment is limited to design verification of the impellers, check for possible frequency interferences that could lead to a high cycle fatigue, and O-ring life analysis. The detrimental effects of corrosion or erosion are not included in the study. Additionally, the characterization of the compressor performance with ageing, and measurements of the casing and piping vibrations, and compressor acoustic mapping are also performed to benchmark the existing performance. The following sections of the paper present the analysis procedures, assumptions, and representative results from selected compressor stages.

COMPRESSOR DESIGN PARAMETERS AND SPECIFICATIONS

The MR-LP 4 stage compressor, with a rated weight flow of 766.34 kg/hr, is a straight through centrifugal unit with horizontal split casing. The tapered shaft (1:16) is made of low alloy forged steel AISI 4340 and has a length of 4,553.9 mm (14.94 ft.). The diffusers are vaneless while the return channels have vanes. The MR-HP 6 stage compressor, with a rated weight flow of 766.34 kg/hr, is a straight through centrifugal unit with vertically split barrel casing. The tapered shaft (1/2" per foot) is made of low alloy forged steel AISI 4340 and has a length of 4,097.0 mm (12.61 ft.). The impellers of both the MR-LP and MR-HP compressors are assembled on the rotor using sleeves and keys. Most of the diffusers and return channels of MR-HP compressor have vanes.

The propane 4 stage compressor has a horizontally split casing. The stepped shaft is made of AISI 4340, with minimum yield strength of 724 N/mm^2, and has a length of 6139.28mm (20.14 ft.). The enclosed impellers, made of AISI 4340, are fabricated with 5-axis milling and welding. The diffusers are vaneless while the return channel and side streams have vanes.

MODAL ANALYSIS

Modal tests (also known as impulse test) were performed on spare rotors of all three compressors in Train 1 and Train-2 to estimate the impeller modal frequencies and to validate the 3D CAD models of impellers. The spare rotors, kept in storage containers, had protective coatings on the impeller surfaces and hence cleansed prior to testing. Note that, while the scanning and modal testing are better performed with the rotor placed on stands, schedule constraints required the task to be performed with the rotors kept inside the bottom half of the containers.

The modal test process involves striking the impeller blade surfaces with a load cell instrumented hammer at various points in a grid mapped on the impeller surface. The impeller response is measured using accelerometers attached on the blade surface at various locations. The impact hammer force and accelerometer response signals were recorded and Fast Fourier Transforms (FFT) were performed for up to 5,000 Hz. Frequency Response Functions (FRFs) are generated using ratio of responses to the applied forces. A modal parameter estimation software, XModal®, processes the experimental data and estimates the impeller natural frequencies, mode shapes, and modal damping ratios. Figure 1 shows photographs of impeller #1 of PR compressor during modal testing. Figure 2 shows the impact locations on the blade and shroud of the Propane compressor impeller #1. The current set of impact points is sufficient to identify mode shapes and frequencies and to compare them to finite element (FE) analysis predictions.

OEM generated CAD models of the impellers were not available. Hence, the authors used laser-scanning technique to generate 3D CAD models of spare impellers. The laser scanning, using a 7-axis Romer® arm, is also performed with the rotors placed inside bottom half part of the containers. The scanner software processes the data and helps generate CAD models from the point cloud. The non-contact scanning avoids creating any surface defects.

Figure 3 displays the frequency response functions (FRFs) generated by the impact and response measurements from Impeller #1 of Propane. The FRF auto power spectrum, showing the distribution of the signal power in the frequency spectrum 0-2000 Hz, displays peaks corresponding to the impeller natural frequencies.

Figure 1. Photographs of Modal Testing. Impeller #1 of Propane Compressor

Impeller CAD models are verified by comparing the test data with FE modal analysis results. Pie sectors, with an angular span of (360°/number of blades), is cut out from the complete impeller model, and a cyclic symmetric modal analysis performed in ANSYS® finite element analysis software. Cyclic symmetric models are computationally more efficient than full models. Note, however, that in reality no impeller blade is identical in geometry due to manufacturing inaccuracies. Hence, different blades will resonate at slightly different frequencies. Following a mesh refinement study, a maximum element size of ~10 mm is chosen for the FE model, while the refined elements at the leading and trailing edge weld locations are of size 2.5 mm.

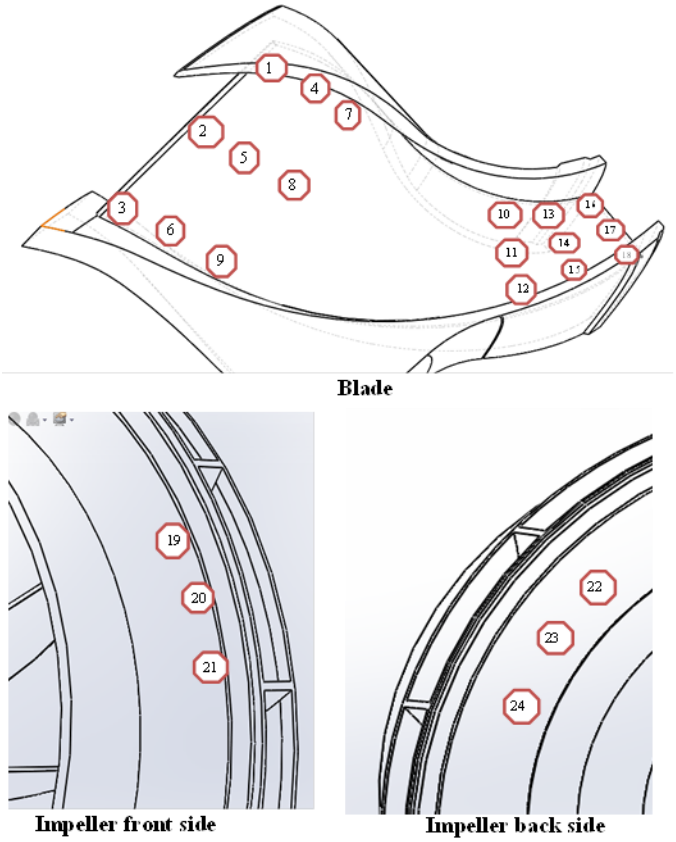

Figure 2. Impact locations on Impeller #1 of Propane Compressor (Typ.)

The smallest impeller natural frequency at 330 Hz (FEA: 352 Hz) is due to a torsional mode. The impeller One and Two-Diameter modes are at 567 Hz (FEA: 576 Hz) and 675 Hz (FEA: 651 Hz), respectively. The frequencies from 765Hz to 811 Hz is due to impeller response. The first blade mode is at 895 Hz (FEA: 910 Hz). Figure 4 shows the experimental and predicted blade mode shapes of Impeller #1 of Propane compressor. The comparable frequencies and mode shapes validate the CAD model. Other remaining 13 impellers of total 3 spare rotors (common between Train-1 and Train-2 Refrigeration Compressors) also show similar results, but not presented here.

The PR compressor consists of 6 inlet guide vanes (IGV) unequally spaced at the inlet. This non-uniform spacing of inlet guide vanes result in the generation of pressure disturbances at mostly 8X, in addition to small amplitude 6X, 4X, and 2X components, as shown by a representative Fourier analysis in Figure 5. Hence, for the fatigue stress analysis of the impeller, the authors focused on the crossings between the 6X and the 8X and corresponding natural modes falling within the operating range of the train.

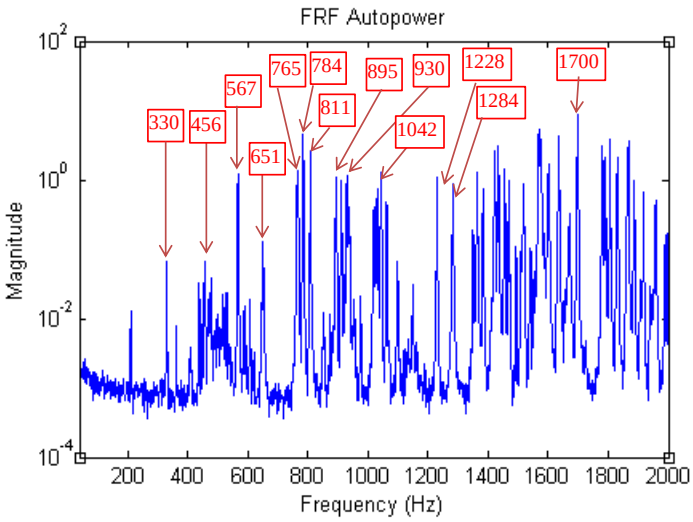

Figure 3. FRF Auto Power. Impeller #1 of Propane Compressor

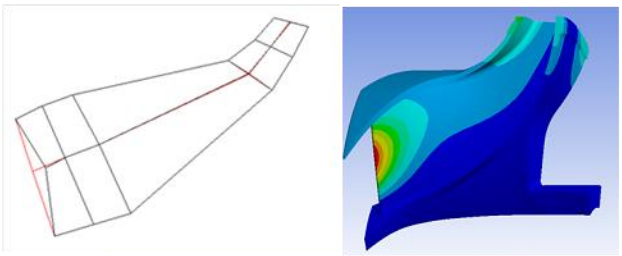

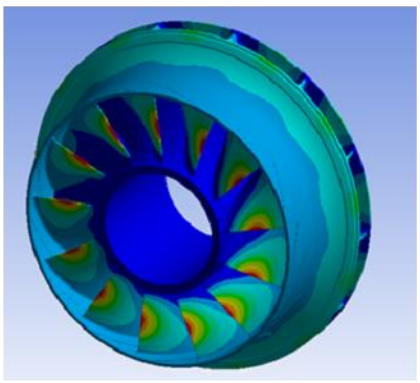

Figure 4. FE Mode shape prediction at 910 Hz. Inset shows comparison of experimental mode shape (895 Hz) and an impeller pie sector

Figure 6 shows the Campbell diagram for PR compressor impeller #1, with impeller natural frequencies on the vertical axis and rotor speed on the horizontal axis. The bold lines are multiples of synchronous speed. In a Campbell diagram, a resonant condition is found when the excitation frequency lines intersect with natural frequency lines in the operating speed range under consideration. For the current impeller, there are natural frequencies near 6X and 8X, and requires further scrutiny. The impeller mode closest to the 6th harmonic is a torsional mode at 330 Hz and not likely to be excited by the alternating pressures on the blade. The FRF autopower spectrum shows small peaks near 456 Hz and 480 Hz (8X), but are not predicted by the FE model. Note also that the FRF peaks near 480 Hz are about an order smaller in magnitude than others, and its excitation is unlikely and hence can be ignored. The probability of resonance due to 12X and 16X excitations are discussed later using an interference diagram (SAFE) diagram. Note that the excitation force amplitudes and aerodynamic damping also influences the resulting stress, and hence these diagrams are only indicative of a potential dynamic interaction.

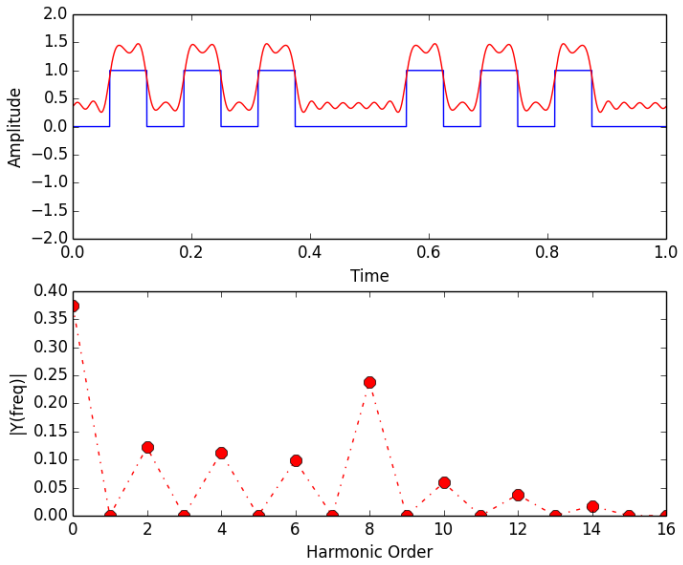

Figure 5. Representative Fourier analysis of pressure disturbances generated by the IGV of PR compressor

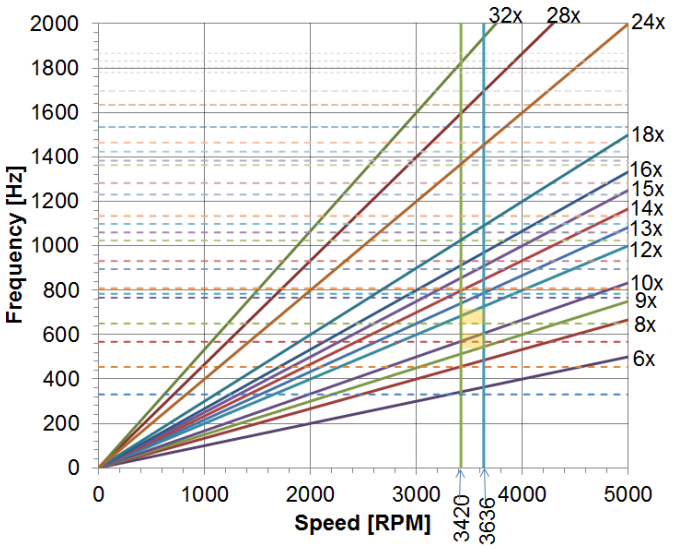

Figure 6. Campbell Diagram for Impeller #1 of PR Compressor

The pressure fluctuations due to upstream vane wakes will induce a circumferential force distribution on the impellers and can excite the disc modes, for instance such as the One and Two-Diameter modes depicted in Figure 7. However, due to phase cancellation, not all modes indicated by the Campbell diagram are usually excited. The interference diagram (SAFE diagram) shown in Figure 8 plots the frequency and mode

shape of the impeller and the excitation harmonics. Typically Campbell diagram shows more resonance conditions than the SAFE diagram. The blue zig-zag line indicates the forcing function harmonic order. The harmonic orders are computed based on the median operating speed of 3540 rpm of PR compressor. A true resonance may occur when the following equations are satisfied

$$(a) \quad |y \times S| \pm |z \times B| = n$$
$$(b) \quad y \times S = h$$
$$(c) \quad fr = y \times S \times w$$

where

B = number of rotating blades
S = number of stationary elements
fr = natural frequency at speed, Hz
h = harmonic of speed
n = number of diameter nodal lines
y and z = integers > 0 (typically only 1 and 2 are important)
w = rotating speed, Hz (rpm / 60)

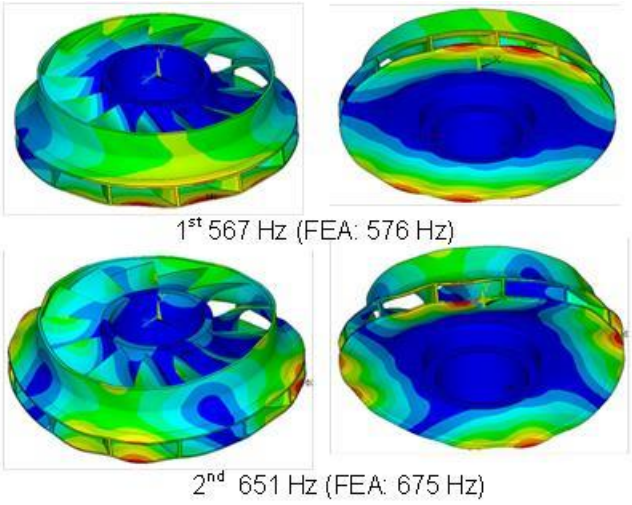

Figure 7. Mode Shapes with One and Two Nodal Diameters

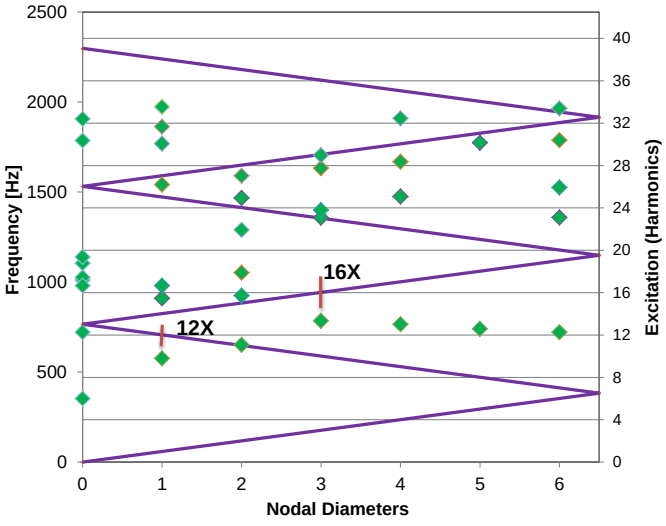

Figure 8. Interference Diagram for PR compressor Impeller #1, 13 blades

For 6X and 8X excitations, and with 13 impeller blades, a 3-diameter mode at 16X is a likely candidate, for instance. However, as shown by the SAFE diagram, the 12X or 16X excitations will not lead to impeller resonance. Impeller excitations due to a combination of higher harmonics (24X, 32X etc.) are not that important. Thus, the SAFE diagram predicts no resonant condition for impeller #1 of PR compressor.

Figure 9 shows the historic trends in the PR compressor strings of Train 1 from March 2008 to March 2014. In general, the operating speed is within 58-59 Hz range. The frequency of shutdowns is not uniform every year. During each start-up and shut-down operation, damages may accumulate on the impellers and may eventually lead to crack generation if it is near the concerning crossings between natural modes and excitations. Typically, this is evident from the interference (SAFE) diagram.

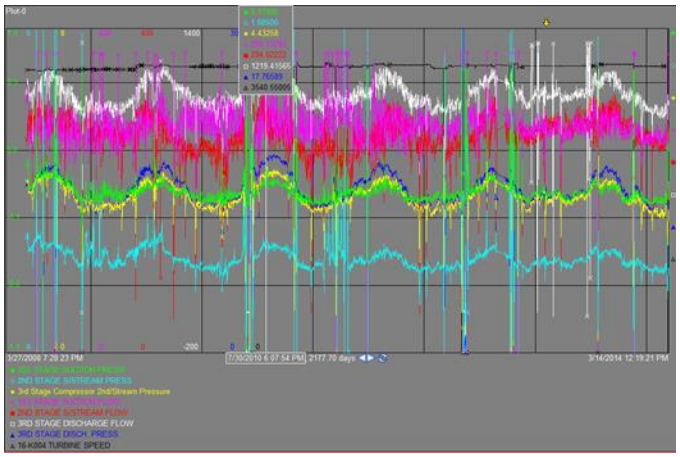

Figure 9. Historic data trends from 03/2008 to 03/2014

Summary: Modal Analysis

Modal testing and analyses were performed and Campbell and Interference diagrams generated for all 14 impellers. For PR compressor, the Campbell diagram and interference diagrams indicate that impeller #2 and #3 of the PR compressor has potential for interaction resonance and hence likely to experience high dynamic stresses. Impellers #1 and #4 of PR compressor do not indicate any likelihood of disc resonance interaction, and hence are relatively safe. For impeller #4 of PR compressor, however, some blade modes in 800 Hz- 1000 Hz frequency range, are likely to be excited by return channel vane wakes.

For MRLP compressor, Impeller #1 shows higher probability of excitation of one of its modes as several natural frequencies exist in the potential vane-blade interaction range. However, for impellers #2, #3, and #4, most of the natural frequencies show sufficient margin against potential integral order excitation frequencies. Impeller #2 of MRLP compressor shows a slightly higher potential for disc resonance interaction, but suitable vane selection in the upstream stage avoids this issue.

For MRHP compressor, all impellers show very low potential for integral order excitation of the blades or any interaction resonance of disc modes. There are sufficient margin between the impeller natural frequencies for safe design of blade-vane combinations. OEMs typically identify the safe

vane wake excitation ranges and select the vane count accordingly.

DYNAMIC BLADE LOADING

One of the major contributors of dynamic blade loading is upstream vane wake. During a single cycle, each impeller blade encounters sudden pressure drops /spikes, as many times as equal to the total number of upstream vanes. This periodic forcing function can generate dangerously high stress levels if any of the impeller natural frequencies are near the operating frequency times the number of upstream vanes, or its integral multiples. Unless there is a resonant condition, the dynamic stress levels in the impellers are usually within allowable limits. A surge or choke operation could, however, cause unexpectedly large stresses. Hence, in addition to the high cycle fatigue analysis, a review of the historic operating conditions is required to verify the departure from the design point. The primary objective of this task is to find the dynamic pressure loads on the reference impeller and scale it suitably, based on operating conditions, for all the impellers (14 Nos.) in the current study.

Performing transient or 'quasi-transient' CFD computations for all 14 impellers would be time and cost prohibitive. As an alternative, CFD flow and pressure predictions available for another same OEM and similar compressor are used for the current study. In a prior study, the authors had computed the pressure distributions in the fourth stage of a similar Propane compressor, say "Reference". The current set of compressors as well as the reference compressor operate in the same speed range of 3420 rpm -3626 rpm. The primary and secondary flow inside a centrifugal compressor is extremely complex, especially due to the considerable variations in geometry, pressure, fluid density, and temperature across various impeller stages. However, since the unsteady pressures (in the rotating frame) on the blade surfaces are mostly caused by the wake flow, once the vane exit flow is characterized, the flow distribution over a 3D impeller blade can be reasonably scaled. Recall that the dynamic blade stresses are due to a combination of operating near resonant conditions and the dynamic pressure magnitude.

In the reference CFD analysis, the overall computational domain includes the return channel, the side stream and the impeller. Figure 10 shows the computational domain used in the analysis. The steady state CFD solution used a "frozen rotor" assumption.

A quasi-transient analysis characterizes the effect of the return channel flow on the impeller blade for various clocking positions. While the analysis captures the transient interaction between the return channel wake and impeller pressure distribution, each analysis is steady state in time. This approach is conservative as it allows the wake to fully develop and over predicts the actual blade loading. Multiple steady-state cases with varying relative position between the return channel vane and impeller blade is used to simulate the transient condition. Six different clocking positions (steady state) between the return channel vane and impeller blade are analyzed in order to obtain a quasi transient behavior. Figure 11 shows a sketch of the impeller blade position with respect to the return channel vane.

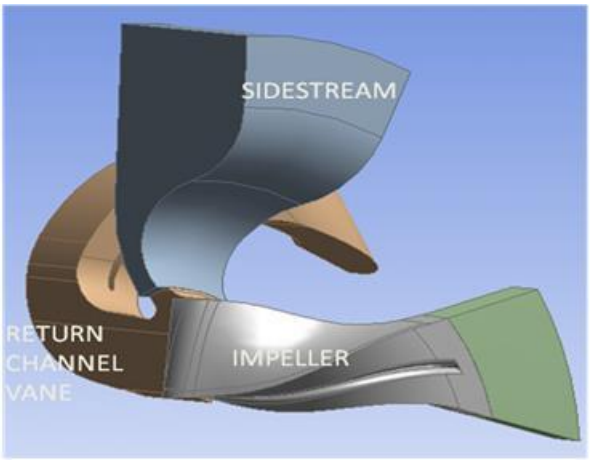

Figure 10. Computational Domain Used for the Analysis

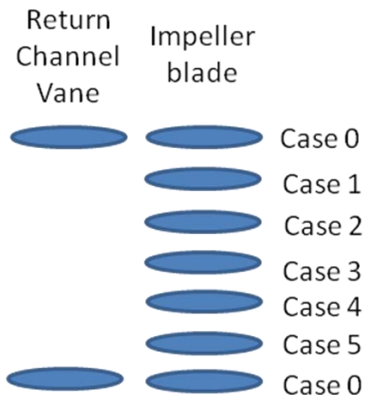

Figure 11. Sketch Showing the Different Clocking Positions Between the Return Channel Vane and Impeller Blade

Vortex flows are generated downstream of an impeller vane, but as the flow pass through the bend of the return channel, the centrifugal and Coriolis forces further change the flow distribution. Secondary flows develop when a moving fluid with a gradient of the reduced stagnation pressure ($P_{rs} = P + 0.5\rho(V^2 - \omega^2 R^2)$) turns around a bend and when rotated about an axis. The flow downstream of the return channel vane is nonuniform, and is dominated by significant jet/wake flow with separation regions that could block up to half the flow passage area. The vorticity kinematics and viscosity determine the wake decay. The flow exiting the return channel vanes show a distinct velocity and pressure profile.

Figure 12 shows the total pressure, in the static frame, at various streamwise locations from the return channel vane exit to the impeller inlet for Case 0 depicted in Figure 11. At the vane exit location, the total pressure of the bulk flow is highest on the pressure side. However, further downstream, the flow with the maximum total pressure gradually moves towards the hub and along the rotor spin direction. Note also the reduction in total pressure due to mixing of the flow with the side flow. The flow distributions in other impeller stages also follow a similar pattern. The flow characteristics indicate that the flow path distance as well as the side stream flow affects the impeller inlet flow.

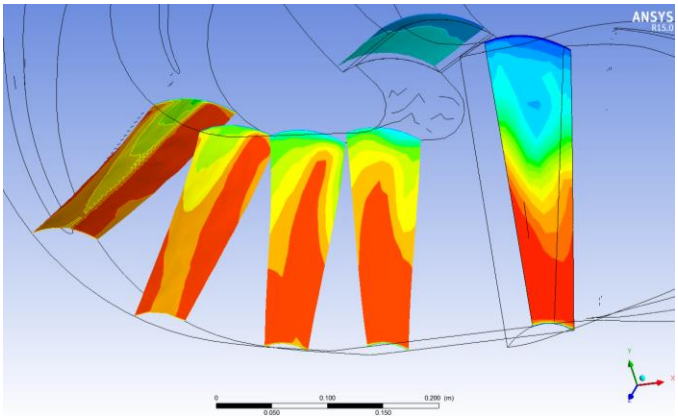

Figure 12. Total pressure (Static frame) at various streamwise locations from vane exit to impeller inlet. Case:0

The pressure loss across the vanes is proportional to the fluid momentum loss in the wake. Japikse [1] presents the total pressure loss coefficient *K*, from an original work by Lieblein and Roudebush [2].

$$K = \frac{\Delta p_0}{0.5\rho V^2}$$

The pressure drop is a function of the pressure loss coefficient, which depends on the wake shape factor, wake displacement, and momentum thickness. The downstream loss is due to a combination of wake profile loss and mixing loss. The pressure loss coefficient is assumed to be comparable for all the impellers. The pressure drop is thus proportional to ρV^2, i.e., proportional to inlet dynamic pressure ($P_T - P$).

The primary flow into the impeller has non-uniform stagnation pressure distribution. As soon as the flow enters the impeller, it is accelerated perpendicular to the primary flow direction. The centrifugal impeller has curvatures in the meridional plane, due to the hub and shroud curvatures, and in the blade-to-blade surface. These curvatures and flow rotations produce secondary flow in the relatively low stagnation pressure fluid. The secondary flow forces the low stagnation pressure fluid to move towards low static pressure region. Note that the wake or boundary layer flow into the impeller will have low relative stagnation pressure. While the blade-to-blade curvature moves the low stagnation pressure fluid to the suction surface, the meridional curvature moves the low stagnation pressure fluid to the shroud. In effect, high stagnation pressures are found on the pressure side and closer to hub.

The current effort is focused on identifying a scheme to map the inlet dynamic pressure distribution to the dynamic blade loading. The net load on the blade is equal to the difference between the forces on the suction and pressure surfaces. The dynamic pressure load is the difference between the maximum and minimum load computed for the various cases: 0-5. As some of the impeller stages in the current study has a side stream, and others not, it is important to notice that the reference CFD analysis was performed with a side stream flow. Hence, while identifying the mapping scheme, the inlet dynamic pressure distributions at two locations are recorded, before and after the side stream location. The former is used to characterize the typical inlet flow for any impeller stage without a side stream, and the latter for a case with a side stream, such as in the reference CFD analysis. Note that this distinction is important due to the significant flow disturbance brought forth by the side stream. Once a mapping scheme is identified from the inlet dynamic pressure distribution (in static frame) to the dynamic pressure loading on the blade (in rotating frame), for finding the dynamic pressure loading on other impeller stages, the inlet dynamic pressure distribution must be suitably scaled up or down. Inlet dynamic pressure scales with ρV^2, using average density and velocity from known design conditions. The mapping scheme also takes into account the fluid rotational effect, from the static to the rotating frames of reference.

The impeller damping is due to a combination of material damping and aerodynamic damping. The material damping arises mostly due to the hysteresis damping inherent to the impeller structure and is proportional to the strain amplitude. Aerodynamic damping arises from the energy lost by the impeller blades in moving the fluid along with the blade surface [3]. From prior SwRI experimental studies and CFD analyses, an aerodynamic damping of 4.29% was estimated for the quasi-transient CFD analysis. Rao [3] and Kammerer [4] shows that aerodynamic damping is linearly dependent on inlet pressures for centrifugal compressors. The original tests were conducted in air and at much lower pressures, though.

Figure 13 shows a typical alternating pressure distribution on a pie-sector model of impeller #1 of PR compressor. Figure 14 displays the alternating pressures for various clocking positions at select locations – blade midspan leading edge, and blade leading and exit ends near the shroud. Note that the blade midspan typically evidences large deflection, while the leading edge weld location near the shroud endures the highest stresses. The alternating pressures at various locations on the impeller blade are not in phase, as seen in Figure 14. However, to be conservative, they are assumed to be in phase in the stress analyses.

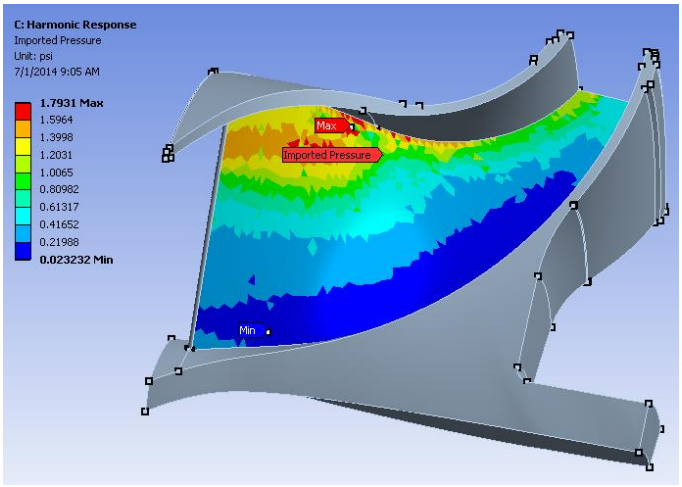

Figure 13. Alternating pressure loading on a pie-sector model of impeller #1 of Propane compressor

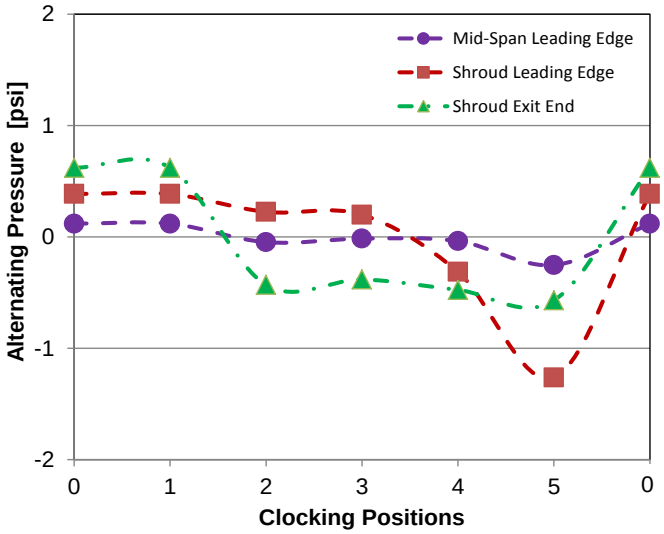

Figure 14. Alternating pressures at select locations on PR compressor impeller #1 blade

MEAN STRESS

The static or mean stress in the impeller is mostly due to its rotation. In the current study, the equivalent mean stress (von-Mises) are estimated using both an elastic stress analysis and an elastic-plastic analysis. The iterative elastic-plastic analysis requires considerable amount of computational resources and hence performed only in certain cases where the high stresses lead to localized yielding. In the analyses, the yield strength and ultimate strength are considered 620 MPa (90 ksi) and 827 MPa (120 ksi), respectively. The API data sheet for PR compressor describes the maximum material yield strength as 931 MPa (135 ksi), and hence the current assumptions are conservative.

Elastic Analysis

In an elastic analysis, irrespective of the material yield strength, the strain recovers once the force is removed from the body. The elastic stretching process does not severe any chemical bonds or cause slipping of atomic layers, and hence is recoverable. Most metals show elastic behavior in accordance with Hooke's Law

$$\sigma = E\epsilon$$

The von Mises yield criterion dictates that material yielding occurs when the distortion energy in a unit volume equals the distortion energy in the same volume when uniaxially stressed to the yield strength. Von Mises stress is defined as

$$\sigma_e = \sqrt{0.5[(\sigma_1 - \sigma_2)^2 + (\sigma_2 - \sigma_3)^2 + (\sigma_3 - \sigma_1)^2]}$$

Here, $\sigma_1, \sigma_2, and\ \sigma_3$ are the principal stresses.

Figure 15 depicts the equivalent mean stresses on the blade at the leading and exit ends. The maximum stresses of 101 ksi (697 MPa) and 185 ksi (1,275 Mpa) at the leading edge weld fillet and the exit end, respectively, are beyond the yielding stress of 90 ksi (620 MPa). In fact, the stresses are larger than the specified maximum yield strength of the material. Clearly, the material undergoes localized yielding. The finite element mesh around the high stress locations on the welds was refined following a mesh dependency study. Traditional approach is to assume that the maximum stresses are limited to the yield strength, especially since the high stresses are present only near the blade surface. However, the authors performed an elastic-plastic analysis to estimate the actual maximum stresses, as described in the next section.

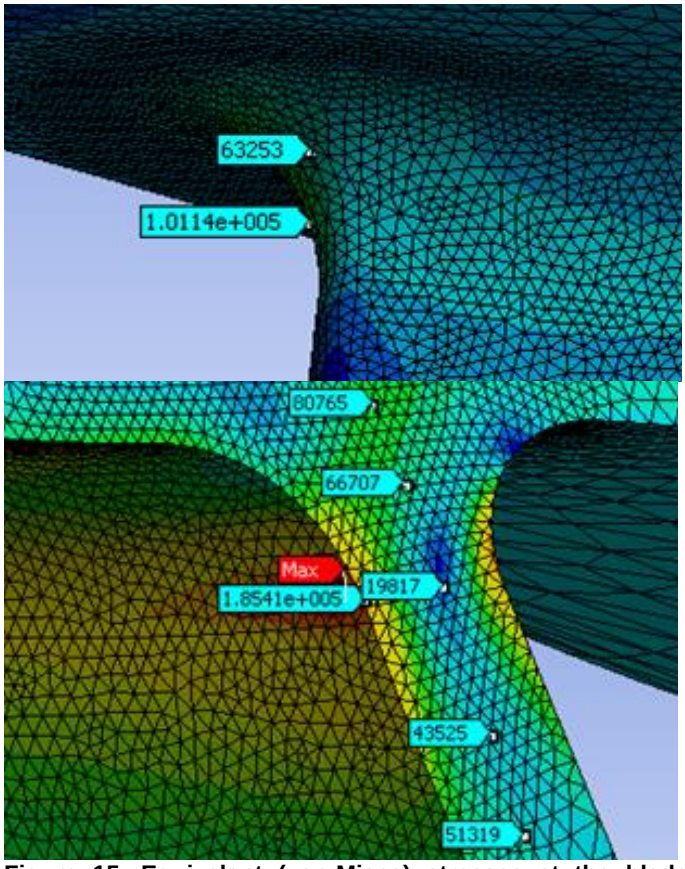

Figure 15. Equivalent (von-Mises) stresses at the blade leading and exit ends. Impeller #1 of PR compressor. Elastic stress analysis

Elastic-Plastic Analysis

In a ductile material, once the stresses exceed the elastic limit, large permanent deformations occur – known as yielding. Any material response beyond yield point is plastic response. During the plastic response, the material absorbs energy resulting in permanent deformations. Plastic deformation occurs mostly due to rearrangement of the atoms in the crystal structure. In the current analysis, a bilinear curve is used to represent the stress-strain behavior. Figure 16 shows the equivalent stresses at the blade leading and exit edges following and elastic-plastic analysis. The maximum stresses in the blade are less than 92 ksi (634 MPa). This indicates that there is a possibility of localized yielding at the weld locations, but no dangerously high mean stresses are present on the impeller.

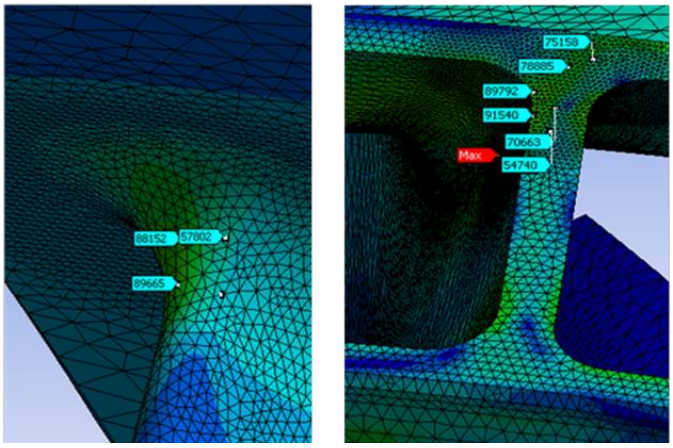

Figure 16. Equivalent (von-Mises) stresses at the blade leading and exit ends. Impeller #1 of PR compressor. Elastic-Plastic analysis

DYNAMIC STRESS

In addition to the mean stresses, dynamic fluid loads induce alternating loads on the impeller. Although small in magnitude compared to the mean stresses, the alternating stresses may lead to fatigue failures if the combined effect of mean and alternating stresses exceeds the material endurance limit. The structural damping available in welded shroud type impellers are rather small, as evidenced from modal testing and from the information available in open literature. From a density scaling of the aerodamping, the estimated total damping for the PR compressor stage 1 impeller is 0.84%. Harmonic Analyses are performed at frequencies of interest using this damping value and scaled dynamic pressure distribution in Figure 13.

Figure 17 shows the maximum stresses in impeller #1 of PR compressor in the frequency range 200-1,000 Hz. The 6X, 8X, and 12X excitation ranges are noted with dashed lines. The peak stress value at the blade leading edge is ~23.7 MPa (3,440 psi). The peak stresses at the exit end is slightly higher at 34.7 MPa (5,038 psi), as shown in Figure 18, than at the leading edge.

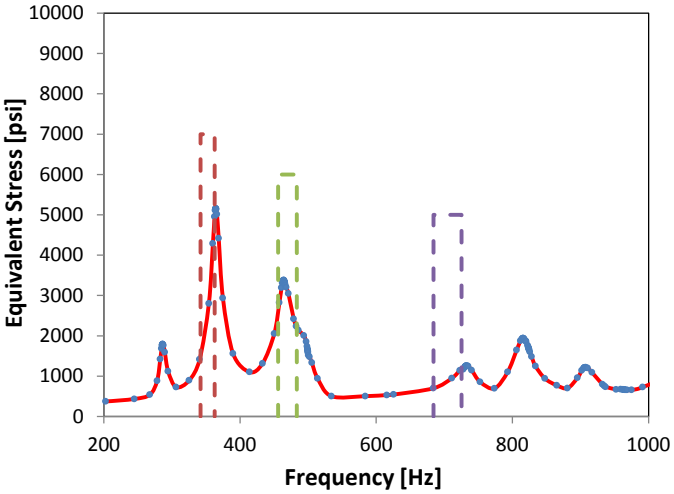

Figure 17. Maximum alternating stress (von-Mises) versus frequency. PR Compressor Impeller #1

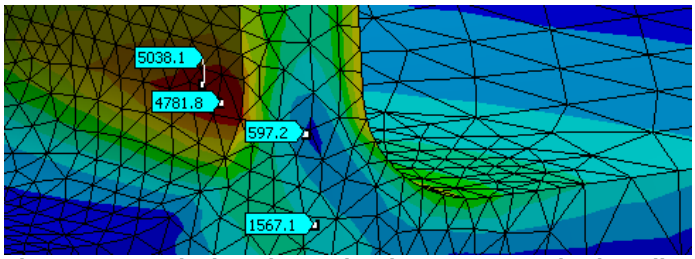

Figure 18. Equivalent (von-Mises) stresses at the impeller exit end for dynamic loads at 364 Hz. Impeller #1 of PR compressor

GOODMAN STRESS DIAGRAMS

Impeller blade fatigue may occur due to large cyclic stresses. The fatigue failure occurs in three phases: crack initiation, crack propagation, and a catastrophic dismemberment of parts. Fatigue failures can be classified as low cycle and high cycle. While the low cycle failures typically involve significant plastic deformation and failure within a limited number of cycles, the high cycle fatigue is characterized by high number of cycles. Most metals have a threshold stress limit known as 'endurance limit' below which fatigue cracks will not initiate. The Goodman diagram is based on endurance and ultimate strength. Any stress below the Goodman line is expected to survive at least 10^9 cycles. Although 10^9 cycles amounts to less than a year of the compressor operation, any stress within the endurance limit is expected to have an infinite life.

As no fatigue test data is available for the current impeller, the test data for a similar impeller [5] is used for the study. The endurance limit line range from a maximum alternating stress of 483 MPa (70,000 psi) at null mean stress to zero alternating stress at the maximum allowable mean stress of 827 MPa (120,000 psi). In addition, a red line with a reduced alternating stress of 276 MPa(40,000 psi) is also shown. The reduced endurance limit, as described in Ref. [5], accounts for statistical variations in the fatigue test data and the differences in surface finish of actual impeller and test specimen. Figure 19 shows a Goodman diagram, maximum alternating stress versus maximum mean stress, for all impellers of the PR compressor. The peak mean stresses in the impellers are at the yield point as localized yielding is expected. The maximum alternating stresses are within the reduced endurance limit. Note that, since a factor of 2 has been included in the dynamic loads to account for possible errors in scaling the pressures, the predicted alternating stresses are conservative. The impeller #2 of Propane compressor shows the highest dynamic stresses of all impellers, indicating that extra care must be taken to ensure no liquid carry in the side stream before the second impeller as the higher dynamic loads could induce excessive stresses at the blade leading edges.

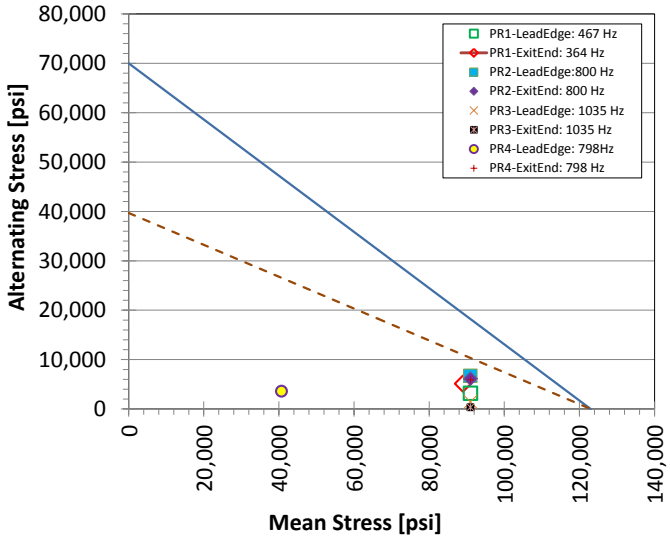

Figure 19. Goodman diagram for Propane Compressor impellers 1-4

Figure 20 depicts the Goodman diagram for all impellers in the MRLP compressor, and Figure 21 shows that for the MRHP compressor. Note that the stress values presented in the Goodman diagrams are worse case conditions, and not likely to be seen during normal operations in the specified operating speed ranges. In general, the mean and dynamic stress combinations are within the reduced endurance limits. Impeller #6 of MRHP compressor shows higher dynamic loads compared to other impellers, but with a relatively lower mean stress value. Recall that the maximum damping was limited to 5% to be conservative.

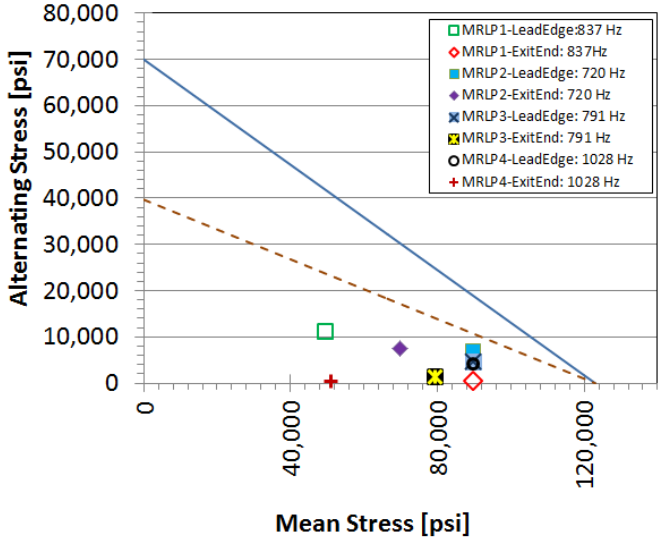

Figure 20. Goodman Diagram for MRLP Compressor, Impellers 1-4

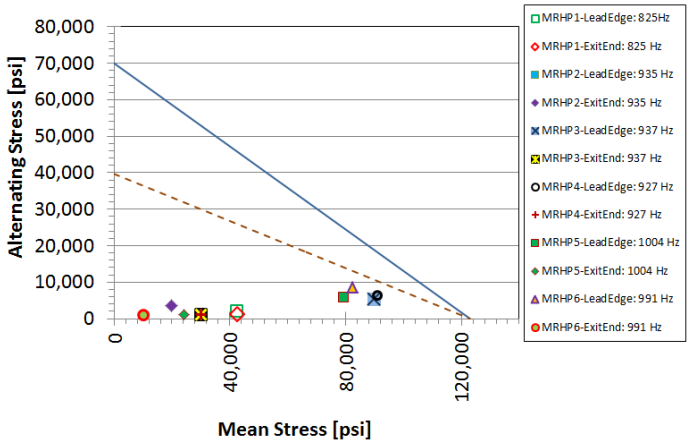

Figure 21. Goodman Diagram for MRHP Compressor Impellers 1-6

Summary: Impeller Fatigue Life Analysis

The mean and alternating stresses in all 14 impellers were analyzed and compared against the impeller endurance limit for infinite life. The mean stresses in the impellers are mainly due to the centrifugal effect of rotation, and often result in localized yielding at the weld locations. The alternating stresses are caused by the flow non-uniformity generated by upstream vane wakes. The Goodman diagrams indicate that the mean and dynamic stress combinations are within the endurance limits for all impellers. PR and MRLP compressor second stages show higher alternating and mean stresses at the blade leading edges. As PR compressor impeller #2 appears sensitive to alternating loads, future operations must avoid stall or choking and any liquid carry over in the side streams. The fatigue stress analyses indicate that, if the OEM specified operating conditions are maintained, the compressors will operate safely until the next major inspection. To this end, the operator has already established stringent choke limits for compressor operation. Additional steps to limit unplanned transients and periodic inspections are being implemented. The analyses have not accounted for any material degradation, fracture initiation, or damages incurred to the impellers during prior operation.

COMPRESSOR AGEING EFFECTS

The rotor response measurements and historic operating characteristics are reviewed to study the effects of ageing in the compressor performance. The flow and pressure ratios are reviewed to check whether any compressor stage had been operating near the choke or surge limits.

Rotordynamic Response

Figure 22 shows the rotor response of Train 1 PR compressor during shutdowns in the years 2010, 2012, and 2013. During 2012 and 2013, two new peaks are found near 2,400 rpm and 3,100 rpm. Note that the overall response also increased from the value in 2010. The Bode plots show that the non-synchronous components have magnitudes larger than the synchronous component as the rotor traverses ~2,400 rpm and ~3,100 rpm. Also, the frequency of the peak at ~2,400 rpm shifted to ~2,800 rpm from 2012 to 2013. At the maximum

operating speed of ~3,600 rpm, the non-synchronous vibration peaks are not present, and hence did not cause any issues during normal steady operations. On further investigation, it was found that the non-synchronous peaks occurred only during unplanned shutdowns (trips) while operating at full load and not during any startups or planned shutdowns. This behavior is attributed to transient surge during full load trips. Further effort is planned to evaluate the anti-surge system and estimate the damages accumulated on the impeller due to repeated transient surge events. The bode and waterfall plot of the rotor responses in Aug, 2014, shown in Figure 23, shows clearly the sub-synchronous components during a transient surge.

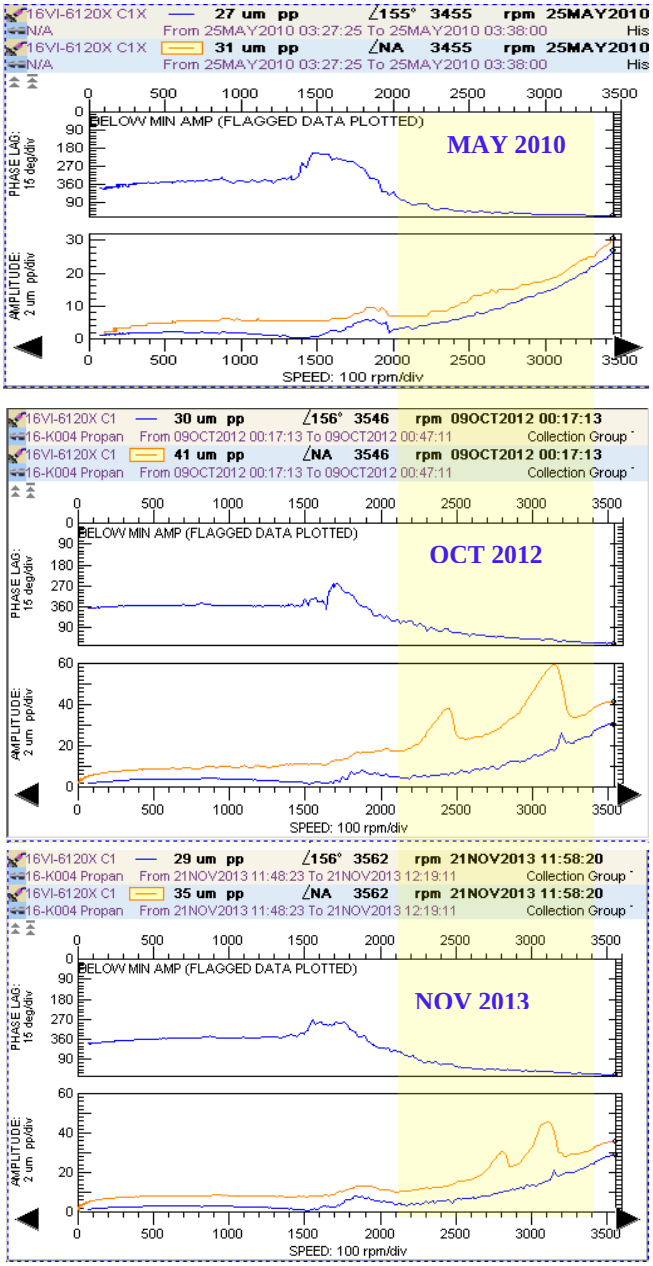

Figure 22. Bode plot of Train 1 Propane compressor rotor horizontal response

Summary: Rotordynamic Response

Based on the rotordynamic response data from 2010 to 2014 for all compressors, the synchronous response is dominant, and any sub- or super-synchronous vibrations are of small magnitude. The bode plot of Train-1 PR compressor shows sub-synchronous peaks during full load trips. This behavior is consistent with transient surge, and likely to induce damages to the compressor components. Further effort is planned to perform impeller stress analysis for transient surge loading to estimate the damages accumulated on the impellers while undergoing repeated transient surge events.

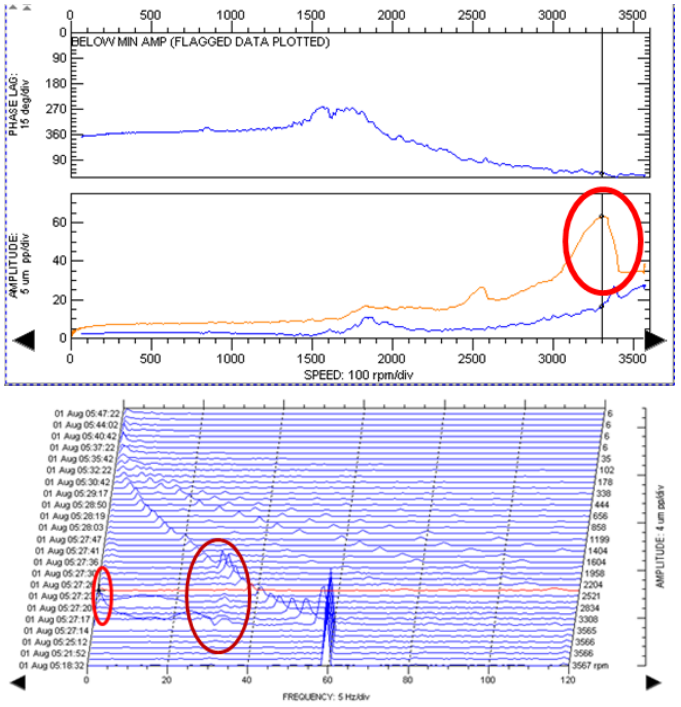

Figure 23. Bode and Waterfall plots of rotor horizontal response measurements in the PR compressor in Train 1, Aug 01, 2014

Performance Characteristics

Figure 24 depicts the discharge pressure versus actual flow of the stage 1 of the propane compressor of Train 1. The measurements are plotted on top of the OEM compressor map. Each of the data point corresponds to one arbitrary measurement point from each month of the years 2008-2014, and not the extreme values during this time period. The steady operating speeds mostly varied between 3,490 rpm to 3,560 rpm. The Propane compressor has two side streams, one after the 1st stage and another after the 2nd stage. Note that the pressure of the side stream between the 1st and 2nd stages mostly varies from 2.2 barA to 3 barA, but occasionally drops as low as 1.8 barA, affecting the stage 1 exit pressures. Nonetheless, the discharge pressure variations are beyond the envelope represented by the OEM performance maps. Extrapolation of the discharge pressure vs volumetric flow curve in Figure 24, corresponding to 3,493 rpm, indicates that the choke instability region starts at a flow rate of 250,000 M^3/hr.

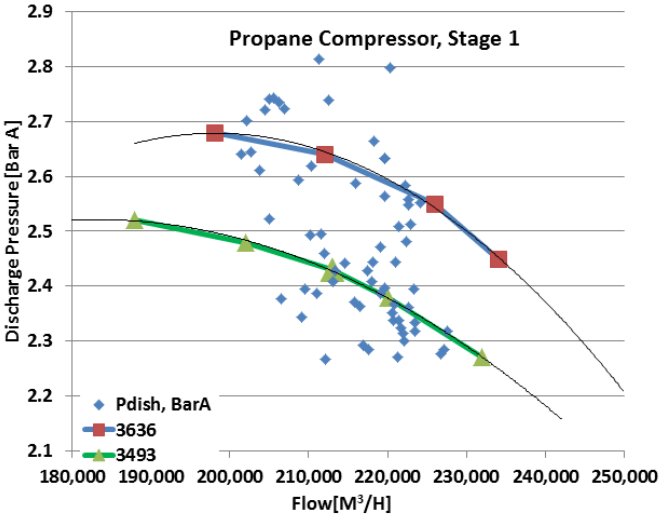

Figure 24. Discharge pressure versus flow (Actual), Propane compressor, Stage 1

Figure 25 shows that stage 2 characteristics are similar to that of stage 1. As with the prior measurements, there is considerable scatter in the discharge pressures, while the actual volume flow rates are near the design point. The flow rates from 2008-2014 indicate that the compressor had been, in general, operating near the peak efficiency point. Figure 26 shows the discharge pressures versus actual flow rates of stage 3 of propane compressors in both Train 1 and Train 2. The operating points of both the compressors show comparable characteristics, with more than expected discharge pressures and volume flow rates, and are near the higher side of the operating envelope. Note, however, that the maximum flow shown by the performance curves are not indicative of a potential choke operation.

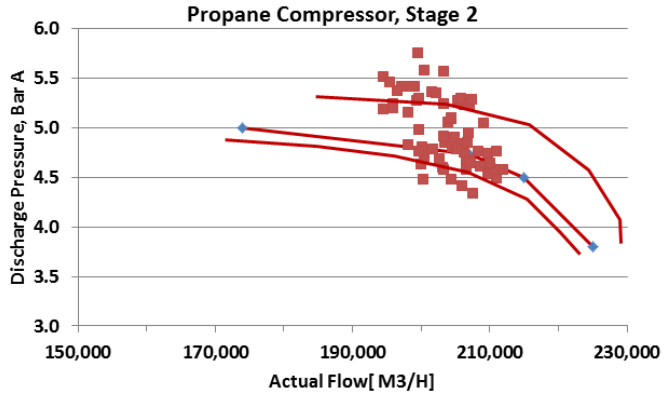

Figure 25. Discharge pressure versus flow (Actual). Propane compressor, Stage 2

Figure 27 shows a comparison of the Propane compressor stage 1 leading edge (LE) incidence angles and flow separation over an extended range to include surge and choke conditions. The incidence angle at the inner radius (IR), outer radius (OR), and midpoint (MID) are shown on the left side vertical axes. The leading edge separation (percentage) is shown on the secondary vertical axis on the right side. It is expected that the high incidence at the leading edge will lead to flow separation and instability; this is experienced at low flow, high pressure ratio conditions as rotating stall, stall, and compressor surge.

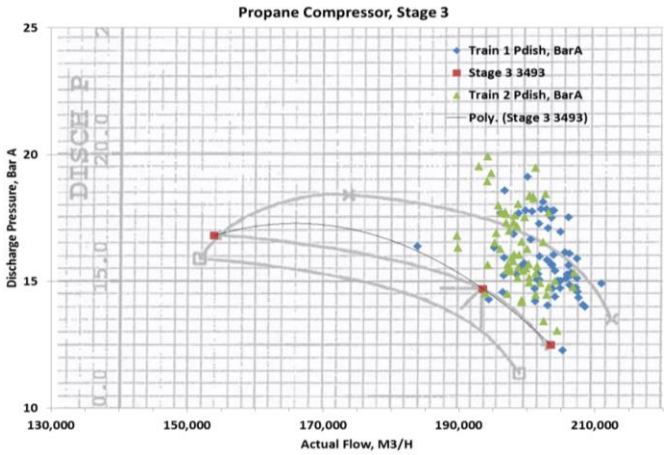

Figure 26. Discharge pressure versus flow (Actual). Propane compressor, Stage 3. Train 1 and 2 data

Almost all reputable compressor manufacturers document their surge conditions and present a safe operating zone; generally, flow margins of 10 to 20% above the estimated surge limit are set as a safe limit. Rotating stall and surge do not occur at flows greater than the design range and some manufactures do not impose a limit on maximum flow, realizing that pressure drops off rapidly and the compressor is no longer useful for its intended purpose as it reaches a choke flow condition. High negative incidence occurs as choke flow is approached which can lead to vortex shedding and blade fatigue especially if resonant conditions are experienced. Excitation forces can also be amplified if the shock boundary moves significantly by the vortex shedding.

Limited information on the compressor design was available; however the data that was available is used to make estimates of a safe choke flow limit by assuming that certain design issues would prevail. An operating curve was estimated based on stage 1 compressor map and extended into the flow ranges where instabilities might be expected, as shown by Figure 27. The ID and OD dimensions were known as were the impeller leading edge angles. What wasn't known were the number of guide vanes and the swirl angle they produced. A simple flow model was developed based on velocity triangles that included the effect of an assumed swirl angle and leading edge incidence and Mach number were calculated vs. flow, as displayed in Figure 28. The objective of the inlet swirl design is to maximize performance at the design point and avoid separation at either extremes of the compressor map. Another main design objective will be to minimize transonic flow over the design range. After several iterations, a swirl angle of -35.6 degrees was found that results in an incidence of -2.3 to -4.3 degrees across the leading edge at design point. At the extremes of the operating range, incidence becomes +4 degrees at min flow, and – 7 degrees at max flow. Only very minimal flow separation is expected at these incidence angles. For volumetric flow rate outside the design range, the leading edge separation rapidly increases beyond 240,000 m^3/h flow rate. As shown in

Figure 24, the historic records of the stage 1 operation shows flow rates in the range 200,000-230,000 m^3/h, which indicates unseparated flow.

Incidence increases to 11.4 degrees at 10% below the minimum flow limit and to 16.4 degrees at 20%; 47% to 77% of the leading edge is in separated flow at these conditions respectively. Similar separation occurs at flows above the design range; -10 degrees occurs at 10% above the maximum the design range and -13 degrees at 20%, while the airfoil is in 100% separation across the leading edge at flows greater than 7% over maximum recommended flow. Maximum relative Mach number and Transonic flow involvement decreases with increasing flow with *Mn* (Machine Mach Number)= 1.05 and 9% transonic in the design range to *Mn*= 1.01 and 3% transonic at flows exceeding 20% of the recommended limit. As discussed earlier, occasionally the first side stream pressures dropped as low as 1.8 barA, which could have dropped the 1st stage discharge pressure to momentarily let some of the flow become transonic. Based on the operating history, such events are rare, with ~ 20 possible occurrences in the last 7 years. A sudden dynamic is not expected as flows exceed the manufacturer's recommendation; damage can occur when periods of vorticity is experienced. The unknown in this case is the character of the vortex shedding excitation, if resonance with the known impeller blading frequencies can occur and if the excitation is sufficient to cause fatigue.

Figure 29 shows the trends in the efficiency vs flange flow for MRLP compressor of Train 1 from 2008 to 2014. There is no significant change in compressor performance in the last 7 years. This is expected as the system operates in a closed loop with no external particle being introduced into the flow. There is, however, a small increase in discharge flow from 2008 to 2014 in Train 1 but not Train 2, possibly due to an increase in balance piston seal leakage.

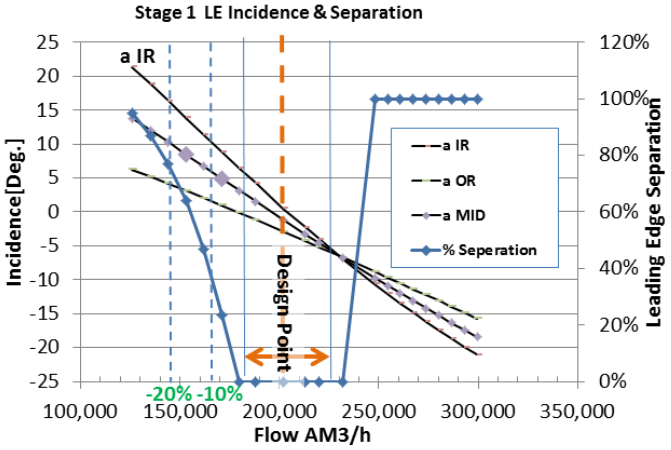

Figure 27. Comparison of Stage 1 LE incidence and Mach Number over an Extended Range to Include Surge and Choke Conditions

Figure 30 shows the efficiency versus flange flow in MRHP compressor of Train 1. As seen in MRLP compressors, the performance characteristics over the years do not show any noticeable degradation or trend, except a small increase in flow rates for the Train 1 compressor. The operating points are within the specified design limits of the OEM, and show no indication of operation in stall or choke conditions.

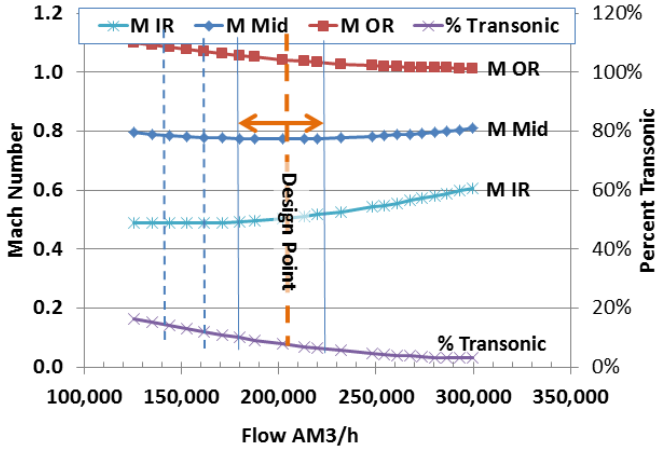

Figure 28. Mach number vs Flow (Actual), Propane Compressor

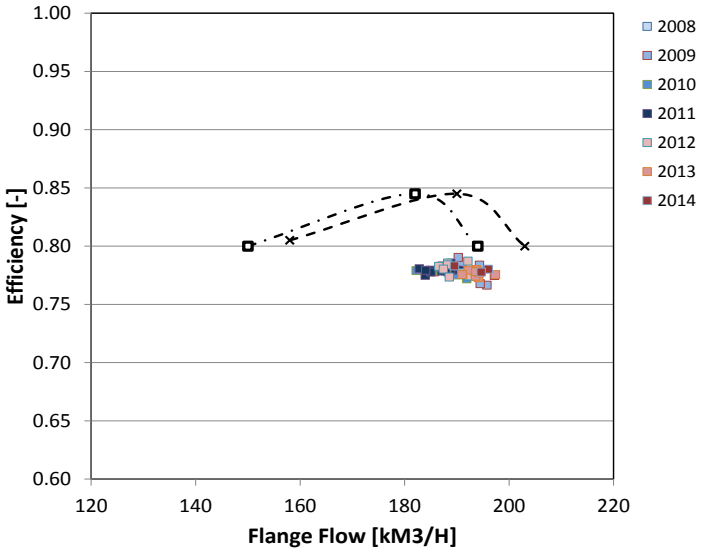

Figure 29. Efficiency vs flange flow (actual) in Train 1 MRLP compressor

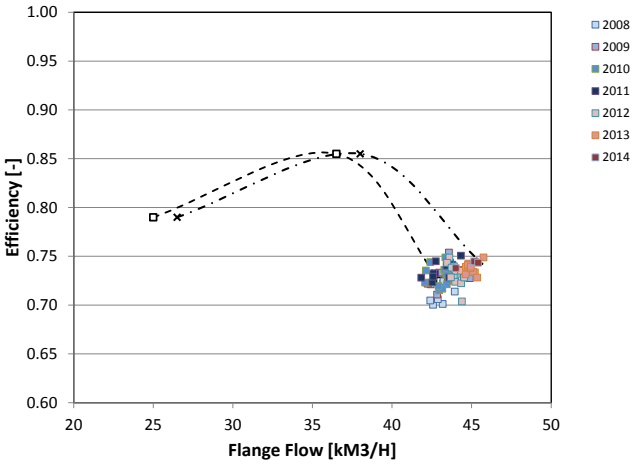

Figure 30. Efficiency vs flange flow (actual) in Train 1 MRHP compressor

Balance Line Pressure and Flow Rates

With aging, the balance piston seals may degrade, resulting in higher seal losses and higher flow to the suction side of the compressor. This in turn increases the impeller volume flow as well as the inlet temperature, both of which cause a decrease in compressor discharge pressure.

Figure 31 shows the balance line pressure and flow rates for PR compressors in Trains 1 and 2. From Feb 2013 to July 2014, there is a small increase in balance line pressure, more in Train 1 than in Train 2. The flow rates, however, show a decrease during the same time. For Train 2 PR compressor, from April to July 2014, the balance line pressure slightly decreased while the flow rates show an increase. The uncertainties and variability in the measurement systems are unknown.

Figure 32 shows the balance line pressures and differential pressures in MRHP compressors of Trains 1 and 2. The balance line pressures increase in both compressors, with the Train 1 compressor showing a more pronounced trend. In general, for all six compressors, the balance line pressures appear to slightly increase during the two years 2013-2014. However, to generate any relevant trends, more data from previous years will be required.

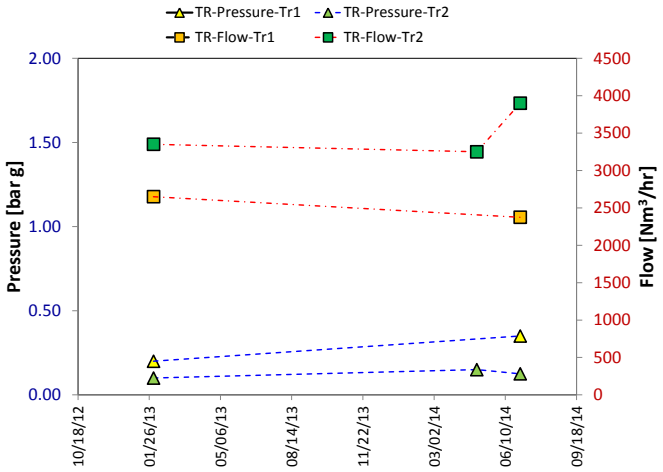

Figure 31. Pressure and flow rates in the balance lines of PR compressors in Trains 1 and 2 from measurements conducted on Feb-2013, May-2014, and July-2014.

Summary: Performance Characteristics

The objective of the task was to identify any trends in compressor performance with ageing, compare the historic performances against OEM compressor maps, and to recommend suitable operating regimes for safe operation in the future. The PR compressor stage-1 discharge pressures show considerable fluctuations, due mostly to the large variations in the first side-stream flow pressures. The actual flow rates are, mostly, close to the design point. However, occasionally, the first sidestream pressure falls as low as 1.8 barA, and could possibly induce transonic flow in stage-1. The choke flow limits determined, based on leading edge incidence, and percentages of flow separation and transonic flows will aid in regulating the operating conditions in the future. The MR compressors show consistent efficiency and pressure ratios, versus actual flow rates, in the last 7 years, and show no noticeable performance degradation. A review of balance line pressure and flow rates show that balance line pressures seem to marginally increase, while the flow rates were either constant or show no clear trends. As the uncertainties in the balance line pressure measurements are unknown, it cannot be ascertained if the changes in the years 2013-2014 are indicative of a larger trend of seal degradation.

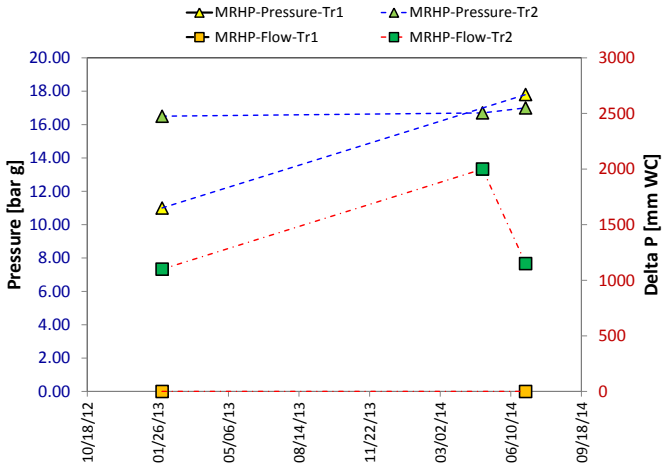

Figure 32. Pressure and flow rates in the balance lines of MRHP compressors in Trains 1 and 2 from measurements conducted on Feb-2013, May-2014, and July-2014.

O-RING LIFE ANALYSIS

The high pressure MR compressor is of barrel type construction and has O-Rings of 7 mm thickness and made of Viton material. O-ring life is affected by various parameters, of which the stress relaxation with age and at high temperature operation is the most important. Stress relaxation is the decrease in stress over time while operating at a constant strain value. In the O-Rings installed in these compressors any degradation due to temperature or oxidation is limited.

The aging behavior of Viton O-ring seals has been investigated by Savannah River National Laboratory (SRNL) for the purposes of sealing the 9975 shipping package [6]. This package stores plutonium in a special materials storage facility. The compression-stress relaxation (CSR) test done in this study is the primary source of predicting the life of the O-ring in the current study. A 90% and 100% loss of compression value was used as a failure criterion. According to the authors [6], the CSR aging model has proved to be conservative compared to the actual time to leakage. Size 2-213 O-ring with a nominal thickness of 0.139" was used in the CSR tests. The thickness is the same as the smallest thickness O-rings used by the compressors. Table 1 shows the reported lifetime of the Viton seals in Ref. [6] and Ref. [7].

Table 1: Comparison of predicted lifetime of CSR model between the SRNL 2009 and 2012 papers at 100% and 90% loss in sealing force

Temperature [Deg. C]	Viton at 100% loss [7]	Viton at 90% loss	% loss not reported [6]
25	3200 years	2200 years	-
79	60 years	35 years	25 years
93°C	-	-	12 years
204	~47 days	~39 days	-
232	~18 days	~15 days	-

As a best estimate, the predicted lifetime plot from the most recent paper [7] has been recreated using a straight edge on an image processing software and fitted in MATLAB using the Arrhenius equation. The Arrhenius equation yields an activation energy of 56.10 kJ/mol for this compression process.

$$k(T) = A.\exp\left(-\frac{E_a}{RT}\right)$$

Here, k(T) is the reaction rate for the process, E_a the activation energy, R the gas constant, T the absolute temperature, and A is a pre-exponential factor.

The fitted plot shown in Figure 33 is for 100% loss of compression, respectively. The Arrhenius equation yields an activation energy of 56.10 kJ/mol for this compression process.

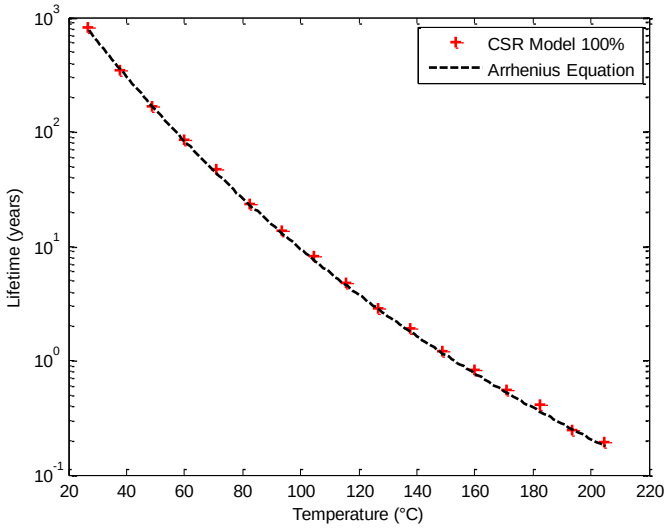

Figure 33: Seal life prediction of Viton GLT O-ring at a 100% loss of compression. *E*: 56.10 kJ/mol, A = 4000, Po/P = 100

The models give a lifetime prediction for a constant temperature. Since the operating temperatures of the compressors vary with time, the best estimate we can get is a monthly average of all of the recorded operating temperatures through a 4-year period. Figure 34 shows the plot for the lifetime for 100% loss of compression at the recorded operating temperatures for the Tr1-MRHP compressor. The lifetime is predicted for each month's average temperature throughout the 4-year period and the average of those lifetimes is taken to be the predicted lifetime of the O-ring seals. The average predicted lifetime for a 90% loss of compression, is 18.9 years. The average predicted lifetime for a 100% loss of compression, is 26.4 years.

Summary: O-Ring Life Analysis

O-Ring life is influenced by several factors, mainly the operating temperature, chemical degradation, loss of compression, and oxidation. For the current application, in an MR atmosphere, and for a maximum temperature of 86 deg. C, thermal degradation was found to be very small and any chemical corrosion unlikely. Any possibility of assembly errors are ruled out. Based on scant published data, an Arrhenius equation based approach was followed to predict the life of the O-Ring. For 100 % compression loss, the predicted life time – based on operating profile of MRHP compressor of Train 1- is 26.4 years. By 18.9 years, the O-Rings would have lost 90% of its compression. As no experimental verification of the O-Ring life has been performed, the current predictive capability is limited, and hence periodic inspection of the compressor for leakage is recommended.

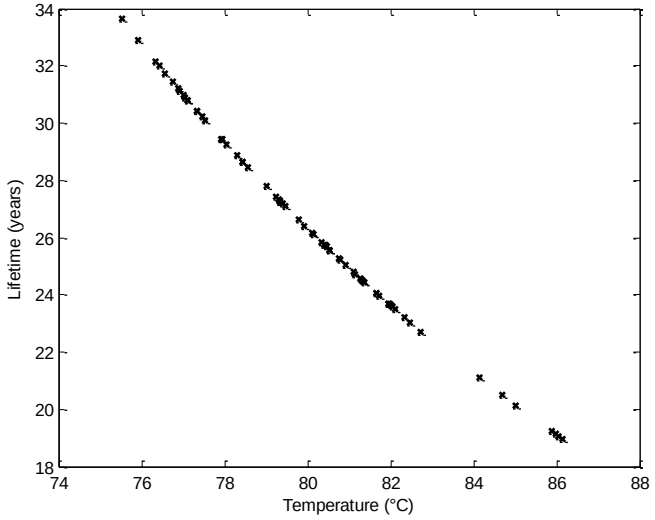

Figure 34: Seal life prediction for 100% loss of compression at recorded operating temperatures for TR1-MRHP. Average Lifetime Prediction: 26.4 years

ACOUSTIC AND VIBRATION MEASUREMENTS

The acoustic and vibration measurements were conducted at all compressor stations to benchmark the current status. In the future, the measurements of compressor vibrations may reveal an anomalous response peak attributable to a defective component. Comparison of the future measurements with current benchmark data will enable easy evaluation of the system performance. This information, however, is not used for the current residual life analysis.

Acoustic levels were measured around trains 1 and 2 at distances of ~ 1m and 2 m to generate acoustic maps. In association with the April 2014 shutdown, scaffoldings were built around the compressors and pipings, which could have affected the measurements. The following figures show the peak acoustic levels (dBa) measured at the MR and PR strings, respectively, of train 1. Train 2 measurements are comparable, but not shown here. In the future, any noticeably different sound level could be due to a sudden change of operating

conditions or any component failure.

Vibration measurements were performed on all compressor pedestals, casing structure, and inlet and discharge piping. shows a velocity probe installed near a piping flange of the PR compressor of train 1. Vibration measurements using velocity probes such as the one shown in Figure 37 provides a vibration spectrum as shown in Figure 38 . The figure shows the spectrum of vibrations at four different locations (on MR-LP compressor of train 1) and show distinct peaks corresponding to various natural frequencies.

Table 2 shows a list of frequencies corresponding to the vibration peaks and their harmonic orders.

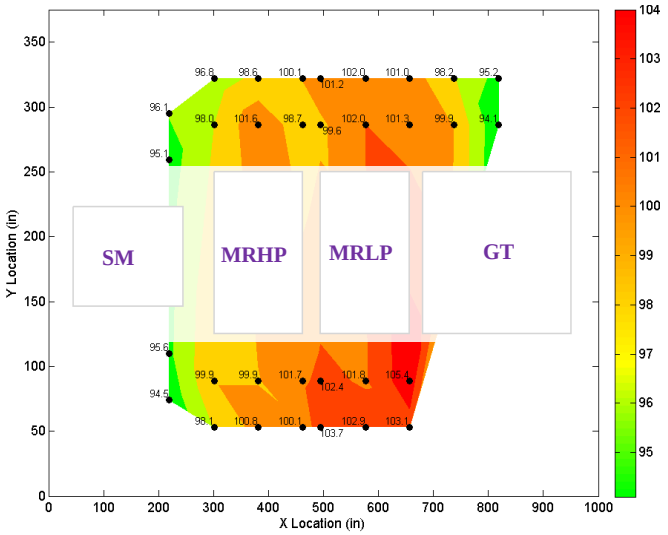

Figure 35. Acoustic Level (dBa) map of MR Compressor String of Train 1

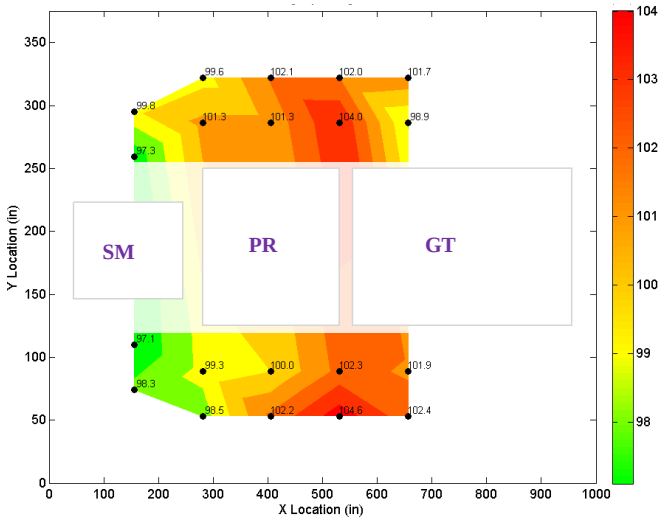

Figure 36. Acoustic Level (dBa) map of PR Compressor String of Train 1

Figure 37. Velocity probe installed near piping flange on the PR compressor of Train #1

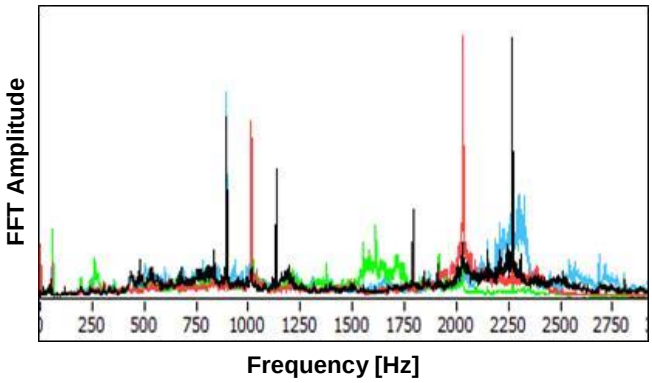

Figure 38. Vibration spectrum on MRLP, Train 1

Table 2. Frequency peaks in measured vibrations in Train 1 propane compressor

Frequencies [Hz]	Harmonic multiple
59	1X
264	Piping response
766	13X
884	15X
1533	26X
1651	28X
1711	29X
1769	30X
2299	39X
2417	41X
2653	45X

CONCLUSIONS

The paper presents the procedures, assumptions, and results of a remaining life analysis work performed for three different types of centrifugal compressors installed in LNG Trains 1 and 2 at RasLaffan Industrial city, Qatar. Laser scanning technique is employed to generate the models for all 14 impellers from spare rotors of the three compressors. Further, modal testing and finite element modal analyses were performed to verify the CAD models. Campbell and Interference diagrams were developed for all impellers to check for potential impeller resonance. A major part of the current study was performing fatigue life analysis, and checking

against their endurance limits. This study repeats the OEM fatigue life design process, and was performed for independent verification. The major conclusions from the study are as follows:

- Based on the identified impeller natural frequencies and potential integral order excitations, most impeller stages have sufficient safety margins.
- Fatigue analyses predict stresses below endurance limits for the conditions analyzed within the design operating range. Some impellers, such as impeller #2 of PR compressor for instance, shows high sensitivity to dynamic loads and could experience dangerously high stress levels. Hence, the operating conditions of the PR compressor must be closely monitored in the future to avoid operation near surge conditions.
- Review of the historic operating conditions indicate that the PR compressor discharge pressures show considerable variability, due mainly to the pressure fluctuations in the side streams. The fluctuations of pressure and flow could lead to transonic flows in the compressor, which could in turn result in higher flow non-uniformities.
- The rotordynamic response data shows that, in general, the synchronous response is dominant, and any sub- or super-synchronous vibrations are small. The bode plot of PR compressor of Train 1 shows non-synchronous peaks during full load trips due to transient surge. Further study is planned to investigate the effects of transient surge on the impeller life to enhance the accuracy of the compressor reliability assessment. Note that, the dynamic simulations may suggest major modifications for seamless operation in the future, which however could be considerably difficult. Nevertheless, the future study will provide a better understanding of the system and enable the operator to modify any operating procedures, if required.
- An Arrhenius equation based approach predicts the O-Ring life for 100% loss of compression at 26.4 years. Periodic inspection of MRHP compressors and checking for any leakage is proposed for O-Ring condition monitoring.
- Future studies could include measurements of noise spectrum and comparison with vibration data, as well as the development of acoustic emission trends.
- In summary, the study indicates that the compressors are adequately designed for infinite fatigue life, and likely to operate reliably until the next major inspection shutdown. The compressor history shows mostly operations within the allowable limits, except during full load trips when transient surge is observed. A study of the cumulative damages due to such events, particularly for the PR compressor impellers #2 and #3, will provide more confidence in the compressor residual life predictions. Development of protocols for ensuring acceptable margins from choke and surge limits and reduction of unexpected shutdowns are underway.

REFERENCES

[1] Japikse, D. (1996). Centrifugal Compressor Design and Performance, Concepts ETI Inc.

[2] Liebleing, S., and Roudebush, W.H. (1956). Theoretical Loss Relations for Low-Speed 2D Cascade Flow, NACA T.N. 3662.

[3] Rao, J. S. (1991), Turbomachine Blade Vibration, John Wiley and Sons, Ltd., New York, New York.

[4] Kammerer, A., Abhari, R. (2008), "Experimental Study on Impeller Blade Vibration During Resonance Part 2: Blade Damping," in Proceedings of ASME Turbo Expo 2008: Power for Land, Sea and Air, Berlin, Germany.

[5] White, N., Laney, S., and Zorzi, C. " RCFA for Recurring Impeller Failures in a 4.7 Mtpa LNG Train Propane Compressor," Proceedings of the Fortieth Turbomachinery Symposium, Sept. 12-15, Houston, TX.

[6] Hoffman, E., Skidmore, E., Daugherty, W., Dunn, A., and Dunn, K. (2009), " Aging and Surveillance of Viton GLT O-Rings in Model 9975 Shipping Packages," Retrieved from http://www.osti.gov/scitech/biblio/95812

[7] Skidmore, E., Daugherty, W., Hoffman, E, Dunn, K, and Bellamy, S. (2012), "Aging Behavior of Viton O-Ring Seals in the 9975 Shipping Package," Retreived from http://www.osti.gov/scitech/biblio/1033337.

ACKNOWLEDGEMENTS

The authors would like to thank the following people for their valuable support and contributions during the study: Dr. Basel Wakileh, Mr. Ruri Novrian, Mr. Moh'd A. Jailani, Mr. Elmer L. Rocacurva, Mr. P. Ramanathan, and Mr. Ouahab Matmour of RasGas company, and Mr. Robert Diaz, Mr. Larry Miller, Mr. David Ransom, Dr. Elliott Bryner, and Mr. Chuong Nguyen of Southwest Research Institute.